Designing multifunctional enzymatic devices for biosensing and chemical conversion

Wei, Z.

Publication date
2025

Chapter 3.

Recyclable and robust optical nanoprobes with engineered enzymes for sustainable serodiagnostics.

This chapter was published as "Recyclable and robust optical nanoprobes with engineered enzymes for sustainable serodiagnostics". Y. Liu[§], Z. Wei[§], M. Damian, X. Zhu, T. Knaus, H. Zhang, F. G. Mutti and F. F. Loeffler, *Adv. Mater.*, **2023**, 35, 2306615. DOI: 10.1002/adma.202306615.

[§] Equal contribution status.

Scan me for the published paper and the movie.

3.1. Abstract

Recyclable fluorescence assays that can be stored at room temperature would greatly benefit biomedical diagnostics by bringing sustainability and cost-efficiency, especially for point-of-care serodiagnostics in developing regions. Here, a general strategy is proposed to generate recyclable fluorescent probes by using engineered enzymes with enhanced thermo-/chemo-stability, which maintains an outstanding serodiagnostic performance (accuracy >95%) after 10 times of recycling as well as after storage at elevated temperatures (37 °C for 10 days). With these three outstanding properties, recyclable fluorescent probes can be designed to detect various biomarkers of clinical importance by using different enzymes.

3.2. Introduction

The diagnostics market has experienced significant growth in recent years, driven by factors such as the increasing prevalence of infectious diseases,[1] the growing demand for point-of-care testing,[2] and technological advances that have enabled the development of more accurate and sensitive serodiagnostics.[3] Fluorescent assays that contain enzyme-based probes have attracted great attention since they are highly selective among biomarkers and are widely used in clinical practice and research, especially for the detection of disease-related small biomolecules (e.g., glucose for diabetes or uric acid for hyperuricemia).[4] However, most of these assays are neither affordable, robust, nor deliverable, which are essential elements of the ASSURED criteria, as defined by the World Health Organization for an ideal diagnostic test for the developing world.[5,6]

Currently available probes are single-use, which not only results in serious waste of resources, but also in high costs for serodiagnosis. Moreover, they are criticized for the difficulty of long-term storage in a warm environment (>30 °C) due to progressive denaturation, which leads to a decrease in their biorecognition ability. Therefore, it remains a global challenge to continuously produce sufficient amounts of probes to meet the diagnostic needs while requiring strict storage at low temperatures, especially in low-resource settings.

3.3. Results and discussion

3.3.1. Rational design of the nanoprobes

Basically, it can be divided into three main parts: fluorescence donor, fluorescence acceptor, and recognition group (Scheme 1). As the diagnostic results depend on the fluorescence signal of the probe, the fluorescence donor should be highly stable, not only in the biofluidic environment but also under repeated excitation; that is, its fluorescence is reliable under various conditions and after recycling. Lanthanide-doped nanophosphors are well-known for their linear-like and non-bleaching fluorescence based on the f-f transition of lanthanide ions.[7] As an intrinsic optical property, the fluorescence of lanthanide mainly depends on the type of dopant and crystal field, and is hardly affected by the environment.[8,9] With a passivation shell coating, the energy migration between emitting dopants and the environment can be further blocked.[10,11] In addition, the lanthanide-doped nanophosphors, especially fluorides, are found to be stable and biocompatible in various biological systems.[12,13] Due to their high signal-to-noise fluorescence and excellent stability, lanthanide-doped nanophosphors are widely used in biological applications, such as in-vivo bioimaging,[14] photodynamic therapy,[15] and optogenetic research.[16] Lanthanide-doped nanophosphors coated with a passivation shell could be suitable fluorescence donors in the probe.

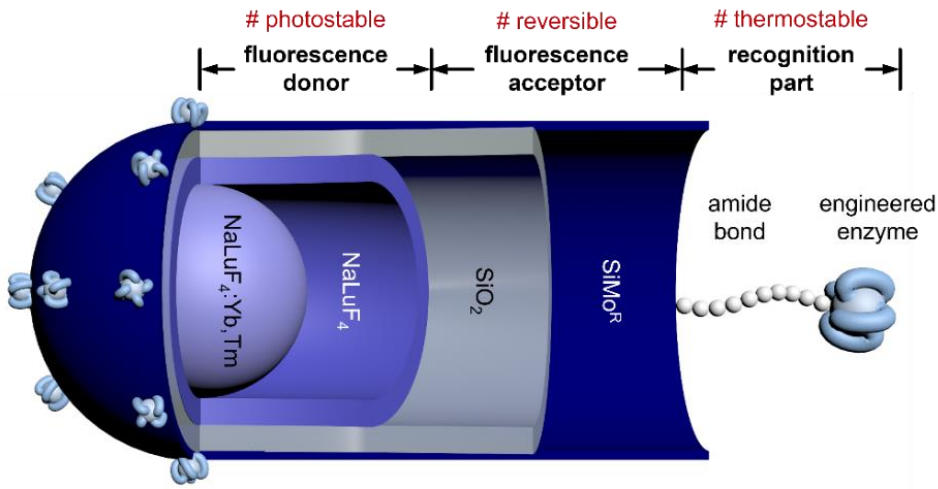

Scheme 1. Rational design of the recyclable fluorescent probe based on engineered enzymes.

As for the fluorescence acceptor, it has to be reversible to meet the recyclability requirement. Typical reversible fluorescence acceptors are organic dyes[17,18] or metal complexes[19,20] that can selectively absorb the fluorescence of the donor in a specific wavelength range. However, most of them are either hydrophobic or unstable under storage, which makes them unfavorable as diagnostic tools applied in aqueous-based biofluids. On the other hand, hydrophilic and reversible inorganic acceptors are more preferable for this specific application. In particular, some of them can grow on the fluorescence donor in-situ, contributing to a stable base for the fluorescent probe. The SiO_2 shell is a widely-used stable base for in-situ growth of various materials and preparation of heterostructures, especially on lanthanide-doped nanophosphors.[21-24] Therefore, a lanthanide-doped and SiO_2-coated nanocomposite with in-situ grown fluorescence acceptors could be a good start to design our fluorescent probe.

3.3.2. Nanoprobes construction and characterization

Based on this, a fluorescent probe of $NaLuF_4$:Yb,Tm@$NaLuF_4$@SiO_2-reduced silicomolybdate (Tm-$SiMo^R$) was designed and constructed. The lanthanide-doped $NaLuF_4$:Yb,Tm core is stable, while the $NaLuF_4$ passivation shell limits the energy loss due to migration from Tm^{3+} to the environment. In addition, the coated SiO_2 is not only a hydrophilic shell, but also provides a stable surface for in-situ growth of $SiMo^R$.[25,26] Therefore, this rationally designed nanostructure will not be easily disassembled or fluorescence quenched in typical biofluidic environments. Morphological, elemental, and crystallographic analyses indicate the successful construction of the probe as designed (Figure 1 and Figure 2).

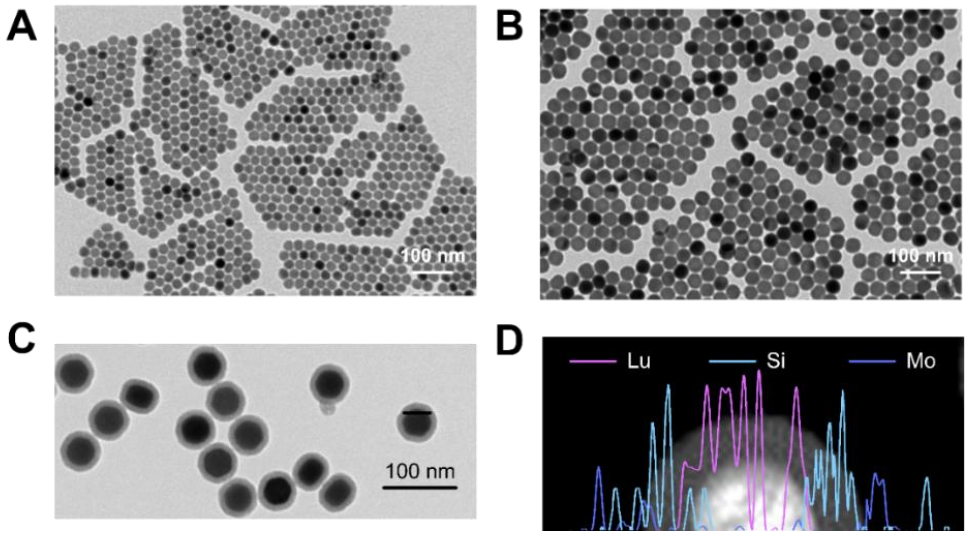

Figure 1. Transmission electron microscopy images of $NaLuF_4$:Yb,Tm (A) , $NaLuF_4$:Yb,Tm@$NaLuF_4$ (B) and the fluorescent probe with the engineered enzymes (C). Electron dispersive X-ray line scan of the fluorescent probes (D).

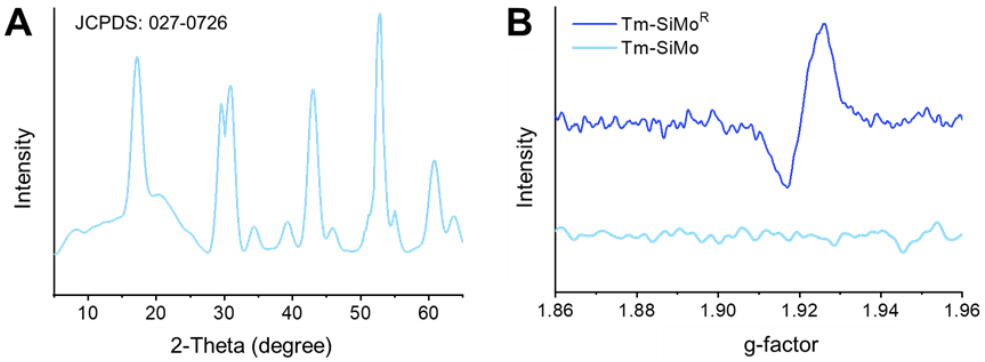

Figure 2. (A) XRD pattern of Tm-SiMo^R. The main pattern can be assigned to the hexagonal phase of $NaLuF_4$ (JCPDS: 027-0726). (B) EPR spectra of Tm-SiMo and Tm-SiMo^R. The g-factor at ~1.92 in EPR spectrum can be attributed to Mo^V in Tm-SiMo^R.

Due to the overlap between the absorption of SiMo^R and the fluorescence of the Tm^{3+}, the fluorescence is quenched by both the inner filter effect and the fluorescence resonance energy transfer pathways (Figure 3A). As the absorbance of SiMo^R originates from the intervalence charge transfer between Mo^V and Mo^{VI}, the addition of H_2O_2 oxidizes Mo^V, thereby weakening the absorbance (Figure 3B and Figure 3C) and, thus, the fluorescence recovers (Figure 3D).

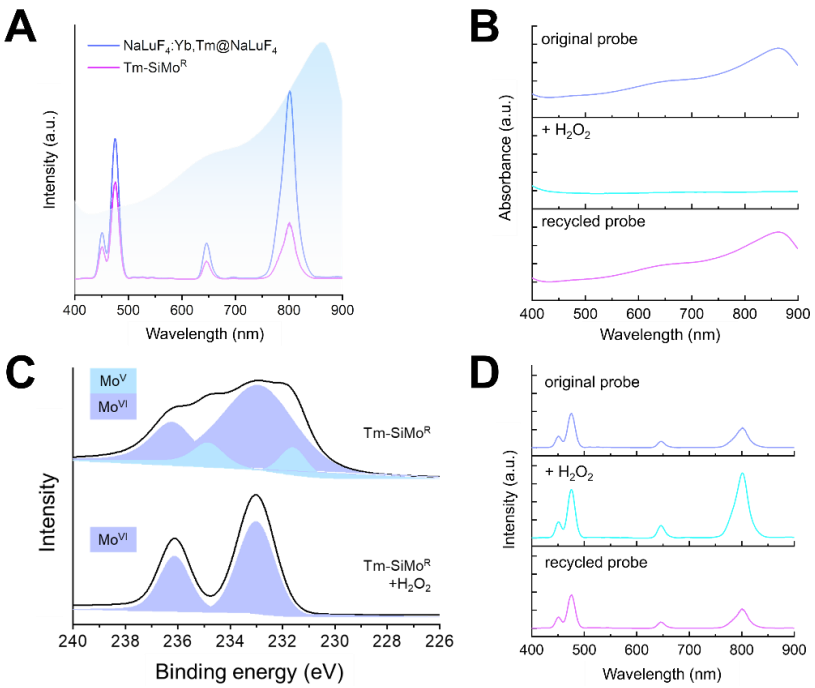

Figure 3. Absorbance and fluorescence spectra of Tm-SiMo^R (A). Absorbance (B) and fluorescence (D) spectra of original Tm-SiMo^R (top), after H_2O_2 addition (center), and after recycling (bottom). Mo_{2p} XPS spectra of Tm-SiMo^R in absence (top) and presence (bottom) of H_2O_2(C).

This oxidation step is finished within 3 min, which enables rapid detection and diagnosis (Figure 4A). It is worth noting that, unlike traditional H_2O_2 fluorescent probes, the oxidation of SiMo^R by H_2O_2 is reversible, allowing the recycling of Tm-SiMo^R after use (Figure 4B). By adding excess ascorbate, the used probes can be reduced, thereby restoring the absorbance and quenching the fluorescence. Therefore, in addition to the reversibility, the Tm-SiMo^R could be used as an H_2O_2 fluorescent probe, often used in clinical practice in combination with a substrate-specific oxidase for biomarker detection.

This oxidation step is finished within 3 min, which enables rapid detection and diagnosis (Figure 4A). The Tm-SiMo^R-BTUO is relatively stable in the standard biological pH range (pH 5–8), which may be attributed to the protection by the functionalization with the modified enzyme (Figure 4B). It is worth noting that, unlike traditional H_2O_2 fluorescent probes, the oxidation of SiMo^R by H_2O_2 is reversible, allowing the recycling of Tm-SiMo^R after use (Figure 4C). By adding excess ascorbate, the used probes can be reduced, thereby restoring the absorbance and quenching the fluorescence. Therefore, in addition to the reversibility, the Tm-SiMo^R could be used as an H_2O_2 fluorescent probe, often used in clinical practice in combination with a substrate-specific oxidase for biomarker detection.

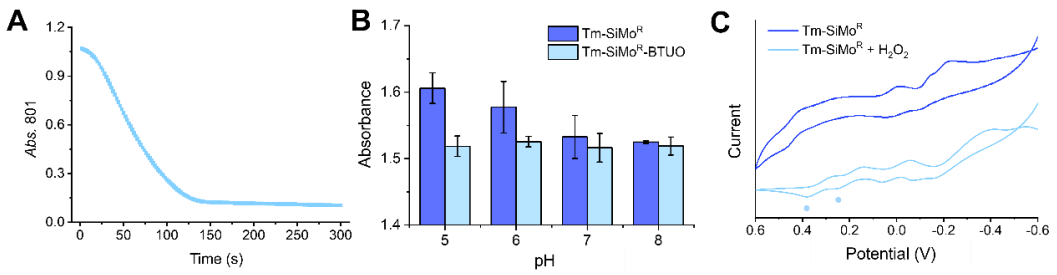

Figure 4. Change of absorbance at 801 nm of Tm-SiMo^R as a function of time in presence of H_2O_2 (A). The absorbance of Tm-SiMo^R and Tm-SiMo^R-BTUO at 801 nm in buffer at different pH values (B). And the CV curves of Tm-SiMo^R in absence (blue) and presence (light blue) of H_2O_2. The two sphere-marked peaks in the CV curves correspond to SiMo, which can be reduced by weakly acidic ascorbate (C).

The last and critical part of the probe is the recognition moiety that is the immobilized enzyme, which determines the ability of the fluorescent probe to recognize biomarkers. In principle, the recognition moiety of the probe could be any oxidase that converts the selected biomarker of clinical importance as the substrate and produces H_2O_2 as the byproduct. Wild-type oxidases are widely used in commercial assays but commonly suffer from moderate stability and catalytic performance under the conditions required for our probe. Therefore, probes based on such oxidases are difficult to store and are unfavorable for providing timely and reliable diagnostic results. Therefore, appropriate selection and engineering of enzymes is important to improve specific properties, such as thermostability through selective mutation and enhanced intramolecular interactions.

3.3.3. The detection performance of nanoprobes with different enzymes

Here, by utilizing an engineered uric acid (UA) oxidase from *Bacillus* sp. (5AYJ, abbr. BTUO, Figure 12 in Method section),[27] a nicotinamide adenine dinucleotide phosphate (NADP) oxidase from *Bacillus subtilis* (1ZCH, abbr. YcnD),[28,29] and an engineered monoamine oxidase from *Aspergillus niger* (2VVM, abbr. MAO-D5, Figure 13 in Method section),[30,31] three fluorescent probes were prepared for the determination of the model disease biomarker UA, the model co-enzyme NADPH, and the model molecular medicine phenylethylamine (PEA). These three model analytes are valuable for early diagnosis of disease (e.g., hyperuricemia and depression), progression monitoring, and evaluation of therapeutic efficacy, respectively. The linear calibration of these three nanoprobes for analyte detection shows the outstanding performance (Figure 5). All three fluorescent probes showed good correlation with the reference 3,3′,5,5′-tetramethylbenzidine (TMB) colorimetric assay currently used in clinical practice (Figure 6 and Figure 14 & 15 in Method section), which not only confirms the generalizability of our strategy, but also validates the practicality of our constructed probes for diagnostic applications.

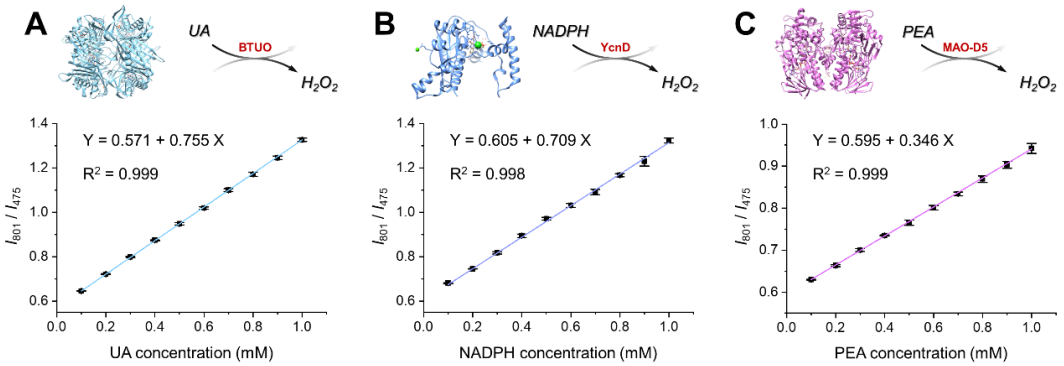

Figure 5. Calibration curves of UA by engineered UA oxidase-conjugated Tm-SiMo^R-BTUO (A), NADPH by NADPH oxidase-conjugated Tm-SiMo^R-YcnD (B), and PEA by engineered monoamine oxidase-conjugated Tm-SiMo^R-MAO-D5 (C). Data are presented as mean ± SD (n = 3).

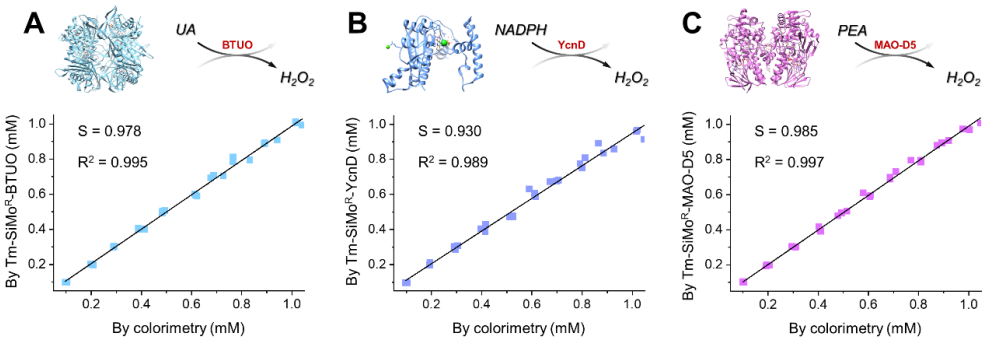

Figure 6. Generalizability of the concept. Quantification of UA, NADPH, and PEA, in 30 buffer samples each, comparing the performance with the reference TMB colorimetric assay. (A) UA by engineered UA oxidase-conjugated Tm-SiMo^R-BTUO, (B) NADPH by NADPH oxidase-conjugated Tm-SiMo^R-YcnD, and (C) PEA by engineered monoamine oxidase-conjugated Tm-SiMo^R-MAO-D5.

3.3.4. The stability and recyclability of the probe

To validate the stability and recyclability of the probe, Tm-SiMo^R-BTUO is selected for the following detailed studies. The BTUO is an engineered enzyme from *Bacillus* sp. TB-90 with substitution of the arginine 298 residue with a cysteine, which enables the spontaneous formation of an inter-subunit bridge, thus improving its thermostability. Therefore, Tm-SiMo^R-BTUO has a prolonged half-life in a warm environment (37 °C) ($t_{1/2}$ = 17.4 days), compared to commercially available probes based on wild-type UA oxidase (4D12, Tm-SiMo^R-wtUO, $t_{1/2}$ = 1.8 days) (Figure 7A). After 10 days of storage, Tm-SiMo^R-BTUO retains a recognition efficiency of 95% in response to uric acid, which is similar to the performance of the freshly prepared probe (Table 1 and Figure 7B).

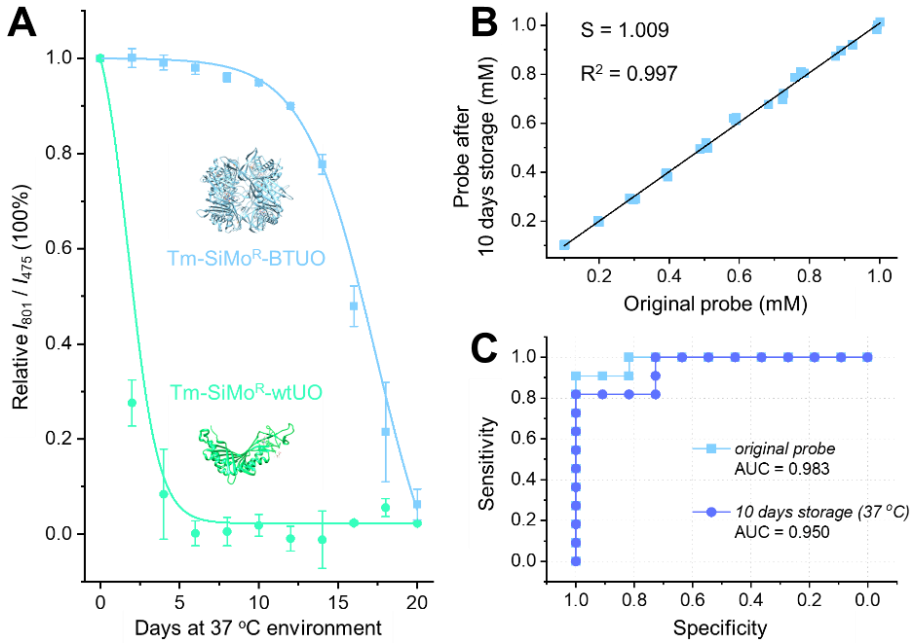

Figure 7. Stability of the Tm-SiMo^R-BTUO fluorescent probe. (A) Relative I_{801}/I_{475} fluorescence ratios of Tm-SiMo^R-BTUO and Tm-SiMo^R-wtUO with addition of 1 mM of uric acid after storage in warm environment (37 °C). (B) Quantification of UA in 30 artificial urine samples. Results obtained by using Tm-SiMo^R-BTUO after 10 days storage in a warm environment (37 °C) are plotted against results obtained using freshly prepared Tm-SiMo^R-BTUO. (C) Receiver operating characteristic (ROC) curve showing the probability for the assay to correctly distinguish between normal and hyperuricemia cases based on the UA content in artificial urine samples determined by fluorescence spectra. Data are presented as mean ± SD (n = 3).

Table 1. UA determination by original probe (A) vs probe after 10 days storage at 37 °C (B). The unit of UA concentration is μM.

Real	Test 1		Test 2		Test 3	
	A	B	A	B	A	B
100	100.9	99.5	100.2	102.6	102.5	104.1
200	200.8	195	196.4	201.2	200.2	196.4
300	287.1	291.9	303	290.1	297	287.7
400	390	393.2	392	396	396.4	380.8
500	510	498	505	520.5	488	494.5
600	583.8	619.8	591	621.6	589.8	610.2
700	727.3	721	683.9	674.8	723.8	695.5
800	760	785.6	776	808.8	784.8	802.4
900	874.8	873	923.4	920.7	891	896.4
1000	995	1001	1001.8	1012.6	993	983

3.3.5. The recyclability of Tm-SiMo^{R}-BTUO

Furthermore, the recyclability of Tm-SiMo^{R}-BTUO was investigated. By using ascorbate in a weak acidic solution, the oxidized SiMo in the probe is reduced. Thereby, the absorbance is regenerated, which can be repeated multiple times (Figure 16 in Method section). Regeneration of the absorbance induces the corresponding change in fluorescence. After 10 cycles, the Tm-SiMo^{R}-BTUO remains stable and applicable as a uric acid fluorescent probe (Figure 8A). The superimposed fluorescence peaks centered at 801 nm ($^{3}H_4 \rightarrow {}^{3}H_6$) for the ten cycles indicate that the fluorescence of recycled probes could be quenched to a similar level, which ensures the reliability of the recycled probe (Table 2 and Figure 8B). Notably, the probe recycled for the 10th time shows comparable quantification performance for uric acid as the original probes (Figure 8C). This still allows for an accurate identification of hyperuricemia cases (>95%) (Figure 8D). In addition to the urine samples, this recycling process also works for human serum and (artificial) sweat, which indicates a wide sample scope for uric acid detection (Figure 17 in Method section). These results show that the Tm-SiMo^{R}-BTUO probe can be recycled by a mild reduction process and it is reliable within certain cycles of use. This can significantly reduce the workload for the production of such probes.

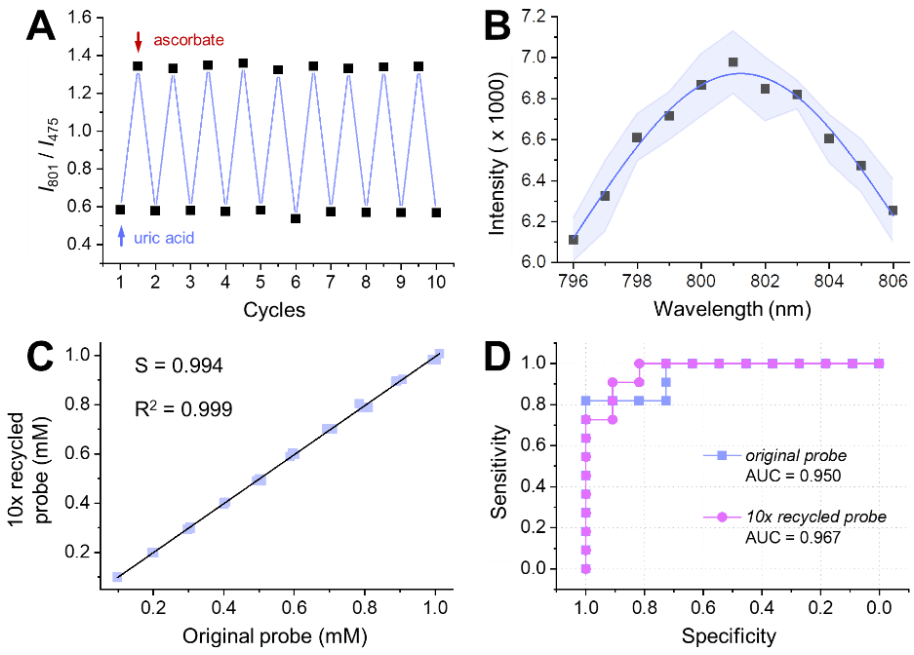

Figure 8. Recyclability of the Tm-SiMo^{R}-BTUO fluorescent probe. I_{801}/I_{475} fluorescence ratios (A) and fluorescence peaks centered at 801 nm (B) for 10 recycling processes. (C) Quantification of UA in 30 artificial urine samples. Results obtained by using 10x recycled Tm-SiMo^{R}-BTUO, plotted against results obtained by original Tm-SiMo^{R}-BTUO. (D) Receiver operating characteristic (ROC) curve showing the probability of the assay to correctly distinguish between normal and hyperuricemia cases based on the UA content in artificial urine samples determined by fluorescence analysis.

Table 2. UA determination by original probe (A) vs 10x recycled probe (B). The unit of UA concentration is μM.

Real	Test 1		Test 2		Test 3	
	A	B	A	B	A	B
100	98.6	98.1	98.9	100.6	98.4	99.3
200	200.8	199.4	201.2	199.8	196.2	199.6
300	304.5	298.5	304.2	302.1	297.6	294.3
400	400	401.2	404.8	402.4	401.2	394
500	493	491	506	490	501	498
600	601.8	596.4	595.2	602.4	588	589.2
700	709.1	700	704.2	701.4	693	702.1
800	810.4	788	795.2	787.2	784.8	802.4
900	907.2	901.8	887.4	894.6	891	896.4
1000	1012	1007	1004	981	993	983

3.3.6. Stability of the probes during the recycling process

Notably, the Tm-SiMo^{R}-BTUO showed both high physical and chemical stability during the recycling process. Due to the mild reduction conditions, the probe maintained its morphological characteristics (Figure 9A), while its dispersibility in aqueous buffer did not change (Figure 9B). In addition, neither Mo leakage nor obvious change in chemical composition were observed in the recycling (Figure 9C and 9D). Moreover, the intrinsic electron structure of the lanthanide ions makes the Tm-SiMo^{R}-BTUO photostable under repeated irradiation cycles (Figure 18 in Method section).

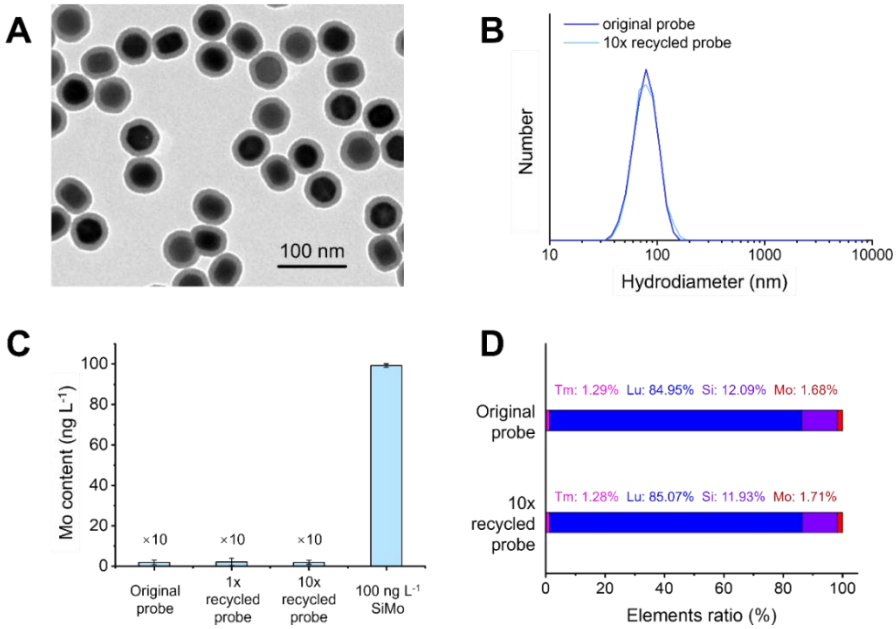

Figure 9. (A) TEM image of Tm-SiMo^{R}-BTUO after 10 recycling steps. (B) Hydrodiameter of original probe and probe after 10 recycling steps. (C) Mo content in the supernatant of original probe, 1x recycled probe, and 10x recycled probe. 100 ng L^{-1} SiMo solution was used as reference. (D) Tm, Lu, Si, and Mo content ratio of original probe and 10x recycled probe.

3.3.7. Fluorescence assay for uric acid detection

Based on the recyclable and thermostable Tm-SiMo^{R}-BTUO probe, a fluorescence assay for uric acid detection and hyperuricemia diagnosis is constructed. After incubation with 96 different test samples (ranging from 0–1 mM concentration of UA) in a 96-well plate, the probes show different visible colors (Figure 10A). Accordingly, the I_{801}/I_{475} fluorescence ratios change and indicate the concentration of uric acid in each well (Figure 10B and Table 7 in Method section). Therefore, the assay can provide either quantitative colorimetric and fluorescence results or qualitative naked eye colorimetric evaluation to meet the needs of different laboratories. By mixing all used probes from different wells together, the probes can be recycled easily within 60 min, including reduction, separation, and re-dispersion steps, to enable the next assay (Figure 10C and Table 6-8 in Method section). The reduction process typically takes 30 min, but could be reduced further if required, since the probes react with the ascorbate within 2 minutes (Movie S1 can be found by scanning the QR code). Therefore, the fluorescence assay can be easily re-used by following this rapid and facile treatment.

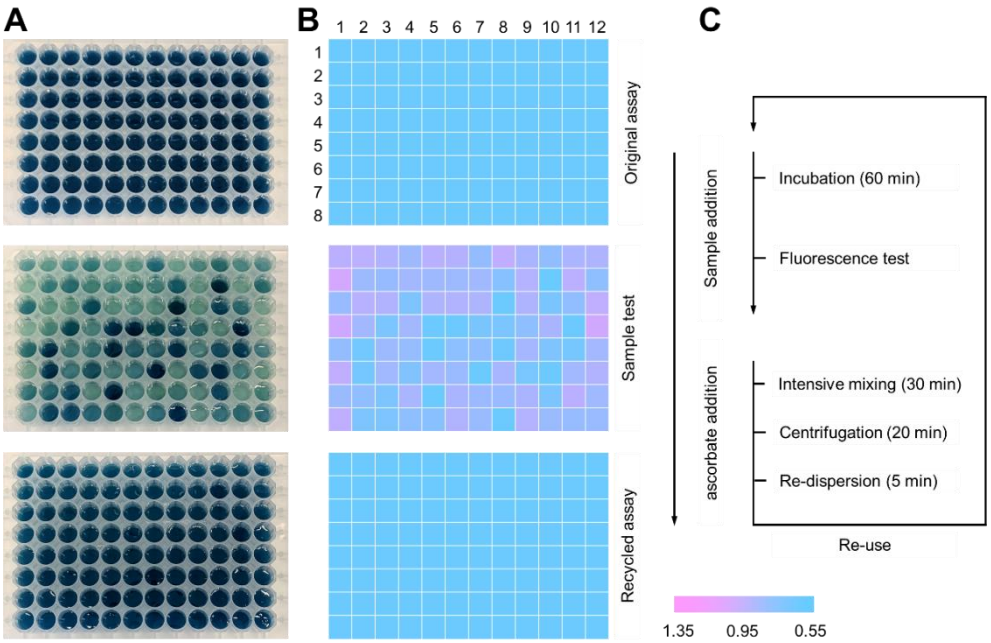

Figure 10. Fluorescence assay in a 96-well plate with recycling, using Tm-SiMo^{R}-BTUO probes. Photographs (A) and I_{801}/I_{475} fluorescence ratios (B) of original Tm-SiMo^{R}-BTUO probes (top), probes after incubation with samples (center), and recycled probes (bottom) in a 96-well plate. Photographs were taken with a smart phone (Google Pixel 5, f/1.7, 1/50, 4.38 mm, ISO134) under warm-white light in the laboratory. Except for cropping, no changes to the images were made. (C) Scheme of the diagnostic and recycling process using the fluorescence assay based on the Tm-SiMo^{R}-BTUO probe.

3.4. Conclusion

In conclusion, we combined materials chemistry with enzyme selection and engineering to construct probes for the determination of biomarkers in biofluids. The probes are recyclable after use and can be stored in a warm environment, due to the reversible oxidation of the polyoxometalate acceptor and the enhanced thermostability of the engineered oxidases. This significantly saves resources, reduces costs, and lowers the requirement for storage, which will improve diagnostics and ultimately the management of various diseases. Apart from the fluorescence, the obvious visible color change may also enable equipment-free colorimetric diagnostics, which would be highly favorable for rapid point-of-care testing. As a result, we provide a general strategy to advance enzyme-based optical diagnostic assays, showing better performance than a current commercial assay (Table 3) and meeting the WHO ASSURED criteria (Affordable, Sensitive, Specific, User-friendly, Rapid and robust, Equipment-free and Deliverable to end-users) for point-of-care diagnostics in the developing world.

Table 3. Comparison of our probe with the commercial Amplex™ Red uric acid assay kit.

Parameter	**Commercial assay kit**	**Our probe**
Detection method	Fluorescence, colorimetric	Fluorescence, colorimetric
Equipment	Microplate reader, spectrophotometer, fluorometer	Microplate reader, spectrophotometer, fluorometer
Protection from light	Necessary	**Not necessary**
Recyclability	No	**Yes (>10 x)**
Storage temperature	< –4 °C	**< 37 °C**

However, there are shortcomings that need to be addressed in the future. First, regarding the accessibility of equipment, besides the fluorescence and colorimetric methods shown here, we will further explore other methods that can provide quantitative results in low-cost settings. For example, the temperature determined by a thermometer can also provide reliable results for diagnosis (Figure 11), and it may be solar powered with appropriate optimization, which is more accessible for developing regions.

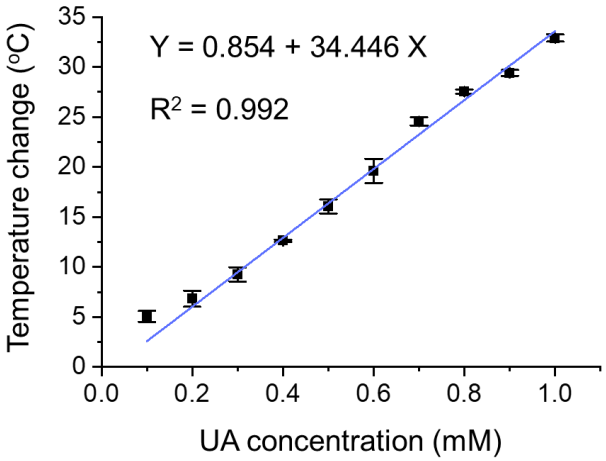

Figure 11. Calibration curve between temperature change and UA concentration by engineered UA oxidase-conjugated Tm-SiMo^{R}-BTUO. The temperature is determined by a digital thermometer (Beurer FT 09) under 808 nm laser irradiation (5 min, 1.0 W cm^{-2}). Data are presented as mean ± SD (n = 3).

Another research priority should be the in-depth exploration of thermostable enzymes for construction of probes. Here, we have shown that the use of engineered enzymes can apparently prolong the stability of probes in a warm environment, which is a good starting point and demonstrates the possibility of obtaining much more robust probes in the future. In addition, although the price of recyclable lanthanide-doped nanoparticles is comparable to traditional dyes (Table 4), the cost of probes could be

further reduced by using cheaper alternative fluorescent cores (e.g., chalcogenide quantum dots and carbon nanotubes) or by exploring bulk synthesis methods. Finally, the study of engineered enzymes should also be considered to broaden the scope of detectable biomarkers, with a particular focus on H_2O_2-producing oxidases (Table 5). In principle, all oxidases could be used to modify the probe, thereby enabling the detection of various biomolecules and the diagnosis of related diseases.

Table 4. Price of lanthanide-doped nanoparticles (No. 926655) and commercial dyes available from Sigma-Aldrich (September 2023). The price of lanthanide-doped nanoparticles and 10-times recycled nanoparticles is highlighted in **boldface**.

Product name (Product No.)	Price (Euro mg^{-1})
IR-780 (No. 425311)	0.09
IR-820 (No. 543365)	0.13
IR-806 (No. 543349)	0.47
10-times recycled nanoparticles (No. 926655)	**3.47**
Indocyanine green (No. 1340009)	3.58
FITC (No. F4274)	4.52
Rhodamine B (No. 79754)	5.52
Rhodamine 123 (No. 83702)	5.97
Rhodamine 6G (No. 56226)	6.06
Lanthanide-doped nanoparticles (No. 926655)	**34.7**
Atto 488 (No. 41051)	244

Table 5. Potentially detectable biomolecules by Tm-SiMoR with corresponding oxidases and related diseases.

Biomolecules	Oxidases	Related diseases
Acetylcholine	Acetylcholine esterase	Cardiovascular diseases, fatty liver, cancer
Cholesterol	Cholesterol oxidase	Cardiovascular diseases
Choline	Choline oxidase	Cardiovascular diseases, fatty liver, cancer
Glucose	Glucose oxidase	Diabetes
Glutathione	Glutathione oxidase	Inflammation, cancer
L-ascorbate	L-ascorbate oxidase	Scurvy
Oxalate	Oxalate oxidase	Lithiasis
Pyruvate	Pyruvate oxidase	Diabetes
Thiamine	Thiamine oxidase	Optic neuropathy
Xanthine	Xanthine oxidase	Hyperuricemia

3.5. Methods

3.5.1. Materials

Lanthanide oxide $LuCl_3$ (99.999%), $YbCl_3$ (99.999%) and $TmCl_3$ (99.99%), 1-octadecene (ODE), H_2O_2 solution, and NH_4F were purchased from Alfa Aesar Chemical Co. Ltd. Other chemicals were purchased from Sigma Aldrich. All chemical reagents were of analytical grade and were used directly without further purification. Deionized water (DI) was used throughout. The artificial urine and sweat samples were prepared according to previous reports, respectively.[32,33] The simulated serum samples were prepared by using purchased human serum with addition of uric acid.

3.5.2. Recombinant enzyme expression and purification

Enzymes sequences and structures are available in the protein data bank (PDB) repository under the accession codes: 5AYJ for BTUO, 1ZCH for YcnD, and 2VVM for MAO-D5.

3.5.3. Expression and purification of engineered urate oxidase from *Bacillus* sp.TB-90 (BTUO)

The synthetic gene encoding for the urate oxidase variant R298C from *Bacillus* sp. TB-90 (BTUO) was subcloned into a pET21a(+) plasmid between NdeI and XhoI restriction sites. The sequence contained a flexible linker (LQNAPAHG) before the XhoI site. *E. coli* BL21(DE3) cells were used as the host organism.

The BTUO expression and purification were performed according to the following procedure. For recombinant expression, 800 mL of lysogeny broth (LB) medium supplemented with ampicillin (100 μg mL^{-1}) were inoculated with 15 mL of an overnight culture of *E. coli* BL21(DE3) cells harboring the desired plasmid DNA. Cells were grown at 37 °C until an OD_{600} of 0.8–0.9 was reached, and the protein expression was induced by the addition of IPTG (0.5 mM). Protein expression was carried out overnight at 25 °C. After harvesting of the cells (4 °C, 10 min, 8944 × g), the remaining cell pellet was resuspended in lysis buffer (50 mM KH_2PO_4, 300 mM NaCl, 10 mM imidazole, pH = 8.0) prior to cell disruption by ultrasonication. The protein purification was performed by Ni-NTA affinity chromatography using pre-packed Ni-NTA HisTrap HP columns (GE Healthcare), previously equilibrated with lysis buffer. After loading of the filtered lysate, the column was washed with sufficient amounts of washing buffer (50 mM KH_2PO_4, 300 mM NaCl, 25 mM imidazole, pH = 8.0), and bound protein was recovered with elution buffer (50 mM KH_2PO_4, 300 mM NaCl, 200 mM imidazole, pH = 8.0). After SDS-PAGE, fractions containing the desired proteins in a sufficient purity (>90%) were pooled and dialyzed against 50 mM K_2HPO_4/KH_2PO_4 buffer (pH = 8.0) overnight and concentrated using Centripreps (Millipore) (Figure 12). The purified enzyme solution was stored at -80 °C as aliquots after shock-freezing in liquid nitrogen.

The final concentration of the protein was determined at 280 nm (ε_{280} = 36390 M^{-1} cm^{-1}). A typical protein yield of 75 mg L^{-1} cell culture was obtained.

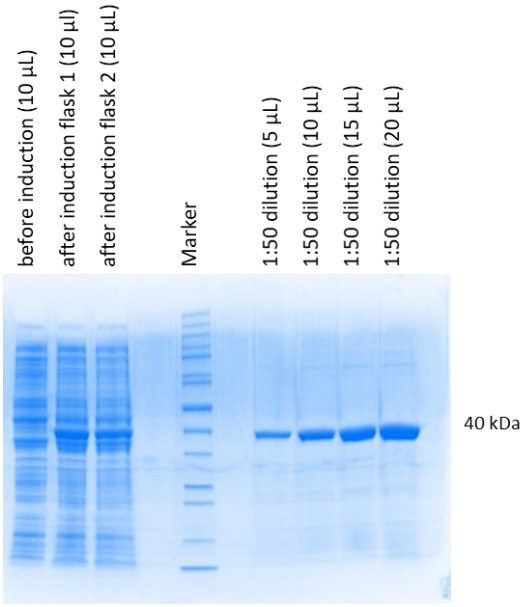

Figure 12. SDS-Page analysis for the expression of UOx R298C (BTUO) and of the purified protein. Marker: PageRuler™ Unstained Protein Ladder (Thermo Fisher Scientific).

3.5.4. Expression and purification of nicotinamide adenine dinucleotide phosphate (NADP) oxidase from *Bacillus* subtilis (YcnD)

Nicotinamide adenine dinucleotide phosphate oxidase, YcnD, was expressed and purified as previously reported by us.[29]

3.5.5. Expression and purification of engineered monoamine oxidase from *Aspergillus niger* (MAO-D5)

E. coli BL21(DE3) cells harbouring a pET28a plasmid encoding for the MAO-D5 enzyme were used to prepare an overnight culture (5 mL LB medium supplemented with ampicillin 100 µg mL^{-1}). Next day, 100 µL of the overnight culture were used to inoculate 10 mL of LB medium supplemented with ampicillin 100 µg mL^{-1}. This secondary culture was grown at 30 °C until the OD_{600} reached ~0.7–1. Next, 8 mL of this culture were used to inoculate the main culture (800 mL of LB medium supplemented with ampicillin 100 µg mL^{-1}) that was grown at 30 °C overnight without the addition of IPTG (i.e., optimized procedure after expression trials using different conditions).

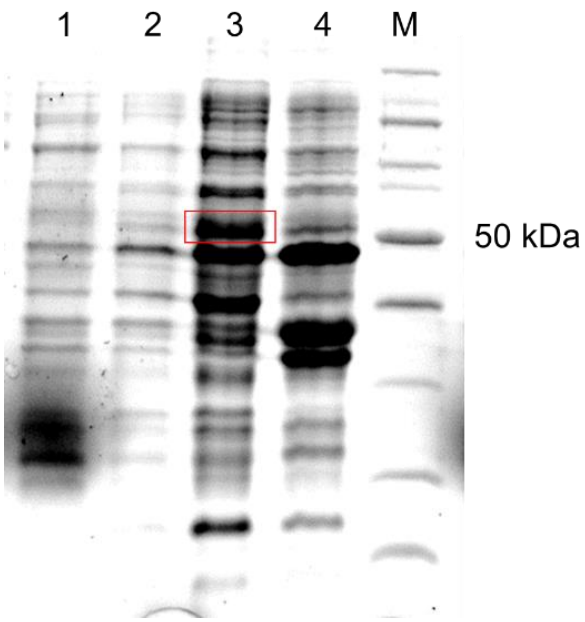

Figure 13. SDS-Page analysis for the expression of MAO-D5. Marker (M): PageRuler™ Unstained Protein Ladder (Thermo Fisher Scientific).

The solubility tests were performed as follows. The samples were centrifuged at 4500 rpm at 4 °C for 15 min. The supernatants were discarded, each pellet was resuspended in 3 mL Lysis buffer and sonicated (5 min of total sonication time, 10 s pulse on, and 10 s pulse off). In total 1 mL of each lysate was centrifuged for 20 min at 4 °C (14534 × g). The supernatants and the pellets were analysed with SDS-PAGE. Sample 1 (1000 µL) was taken before overnight expression from the secondary culture when OD_{600} was 0.92. Sample 2 (1000 µL, after 1:5 dilution) was taken after overnight expression from the main culture in absence of IPTG. Samples 3 and 4 were taken from the soluble and insoluble fractions, respectively, after disruption of the cells. Based on the reported molecular weight of MAO-D5 (MW: 55.617 Da), it was observed that although the expression of the enzymes seems to be low (Figure 13, line 2), the enzyme was found to be in the soluble fraction (Figure 13, line 3). Moreover, no enzyme is present in the insoluble fraction (Figure 13, line 4). Attempts of purification of MAO-D5 with Ni^{2+}-affinity chromatography revealed that the enzyme only eluted in the flowthrough. Due to this fact and the low expression level, the crude lysate was used in this work.

3.5.6. Synthesis of $NaLuF_4$:Yb,Tm@$NaLuF_4$

In a typical experiment, a mixture of 1 mmol $LnCl_3$ (Ln: 80%Lu, 19%Yb, 1%Tm), 15 mL oleic acid (OA), and 15 mL ODE are added into a 100 mL three-necked flask. Under the vacuum, the mixture is heated to 160 °C to form a clear solution, and then cooled to room temperature. After the solution has cooled down, 0.025 mmol NaOH (0.1 g) and 0.04 mmol NH_4F (0.1481 g) are added into the flask directly and stirred for 30 minutes. The solution is slowly heated under gentle stirring, degassed at 100 °C, and then heated to 300 °C and maintained for 1 hour under Argon atmosphere. After the

solution is cooled to room temperature, the $NaLuF_4$:Yb,Tm are separated via centrifugation (11180 × g) and washed with ethanol/cyclohexane (1:1 v/v) three times. The product is stored at room temperature in cyclohexane.[34] The $NaLuF_4$:Yb,Tm@$NaLuF_4$ are obtained by a similar procedure by using different lanthanide sources ($LuCl_3$ for $NaLuF_4$:Yb,Tm@$NaLuF_4$).

3.5.7. Synthesis of $NaLuF_4$:Yb,Tm@$NaLuF_4$@SiO_2

In a typical experiment, 250 μL $CHCl_3$ containing 5 mg as-prepared $NaLuF_4$:Yb,Tm@$NaLuF_4$ are mixed with 2.5 mL hexadecyltrimethylammonium bromide (CTAB) solution (37.5 mg mL^{-1}) under sonification for 5 minutes. The mixture is transferred to a 100 mL three-necked flask and heated in a 60 °C water-bath to form a clear solution. Then, 22.5 mL DI water is added and the solution is heated to 70 °C before 0.3 mmol NaOH (0.012 g) is added directly. After 20 minutes stirring (600 rpm), 120 μL tetraethyl orthosilicate (TEOS) is dropped slowly and 0.5 mL ethyl acetate is added within 30 seconds. Finally, the solution is continuously stirred in a 70 °C water-bath for another 3 hours to enhance the stability of the SiO_2 shell. After the solution has cooled to room temperature, the $NaLuF_4$:Yb,Tm@$NaLuF_4$@SiO_2 are separated via centrifugation (11180 × g) and washed with ethanol three times, respectively. The as-obtained $NaLuF_4$:Yb,Tm@$NaLuF_4$@SiO_2 is then suspended in 50 mL ethanol containing 0.3 g NH_4NO_3 upon stirring for 1 hour at 60 °C. The CTAB-removed $NaLuF_4$:Yb,Tm@$NaLuF_4$@SiO_2 are separated via centrifugation (11180 × g) and washed with ethanol three times.[35] Then, $NaLuF_4$:Yb,Tm@$NaLuF_4$@SiO_2 are dispersed in 10 mL of ethanol and 0.24 mL of (3-aminopropyl)triethoxysilane are added. After 12 hours refluxing at 80 °C in a water bath, the amino-modified $NaLuF_4$:Yb,Tm@$NaLuF_4$@SiO_2 are separated via centrifugation (11180 × g) and washed with ethanol three times. Afterwards, amino-modified $NaLuF_4$:Yb,Tm@$NaLuF_4$@SiO_2 are dispersed in 10 mL DI water, with dropwise addition of 5 mL N,N-dimethylformamide (DMF) containing 20 mg oxalic acid, 80 mg 1-(3-dimethylaminopropyl)-3-ethylcarbodiimide hydrochloride, and 50 mg N-hydroxysuccinimide. After 12 hours of continuous stirring at room temperature, the carboxyl-modified $NaLuF_4$:Yb,Tm@$NaLuF_4$@SiO_2 are separated via centrifugation (11180 × g) and washed with water three times. The product is stored at room temperature in DI water.

3.5.8. Synthesis of $NaLuF_4$:Yb,Tm@$NaLuF_4$@SiO_2-SiMo (Tm-$SiMo^R$)

In a typical experiment, 1 mL H_2SO_4 is added to 5 mL DI water containing 5 mg as-prepared carboxyl-modified $NaLuF_4$:Yb,Tm@$NaLuF_4$@SiO_2. After stirring at room temperature for 10 minutes, 0.5 mL DI water containing 0.05 mmol $(NH_4)_2MoO_4$ (0.0098 g) is added and the mixture is then dried for 4 hours at 100 °C to stabilize the SiMo modification. The Tm-SiMo are separated via centrifugation (11180 × g) and

washed with DI water three times. Then, 5 mg as-obtained Tm-SiMo are dispersed in 5 mL DI water containing 20 mmol ascorbic acid (352 mg) upon stirring for 20 minutes at room temperature. The Tm-SiMo^{R} are separated via centrifugation (11180 × g) and washed with DI water three times. The product is stored at room temperature in DI water.[25]

3.5.9. Modification of enzyme on Tm-SiMo^{R}

In a typical experiment, 10 mg BTUO is dissolved in 10 mL DI water, with dropwise addition of 5 mL DMF containing 10 mg Tm-SiMo^{R}, 40 mg 1-(3-dimethylaminopropyl)-3-ethylcarbodiimide hydrochloride, and 25 mg N-hydroxysuccinimide. After 12 hours of continuous stirring in an ice bath, the Tm-SiMo^{R}-BTUO are separated via centrifugation (11180 × g) and washed with water three times. The product is stored at -80 °C in DI water. The Tm-SiMo^{R}-YcnD and Tm-SiMo^{R}-MAO-D5 are obtained by a similar procedure by using different enzymes (YcnD for Tm-SiMo^{R}-YcnD and MAO-D5 for Tm-SiMo^{R}-MAO-D5).

3.5.10. Characterization

The morphology of the nanostructures formed by the layer-by-layer coating procedure are determined using a FEI Tecnai G^{2}F30 transmission electron microscope (TEM). Samples of the above nanoparticles are drop casted on the surface of a copper grid. Energy-dispersive X-ray (EDX) line scan of the samples is performed during TEM measurements. UV-vis-NIR absorbance spectra are determined on a Shimadzu UV3600 UV-vis-NIR spectrophotometer. Powder X-ray diffraction (XRD) pattern is measured with a Brucker D8 advance X-ray diffractometer from 5° to 70° (Cu Kα radiation, λ = 1.54 Å). X-ray photoelectron spectroscopy (XPS) spectra are performed on Thermo escalab 250Xi. The sample for XRD and XPS determination is previously dried in nitrogen atmosphere at 100 °C. Electron paramagnetic resonance (EPR) spectra are determined on a Bruker A300 electron paramagnetic resonance spectrometer. Cyclic voltammetry (CV) curves are obtained by electrochemical station (Chenhua Instruments Co. CHI600). A three-electrode system is made up of a glassy carbon electrode (GCE, 3 mm in diameter) as the working electrode, an Ag/AgCl electrode (saturated KCl) as reference electrode, and a Pt wire as counter electrode. The fluorescence spectra are taken on a FLS980 lifetime and steady state spectrometer (Edinburgh Instruments) equipped with an external 0–7 W 980 nm adjustable laser as the excitation source.

3.5.11. Calibration curves for uric acid (UA), NADPH, and phenethylamine (PEA) determination

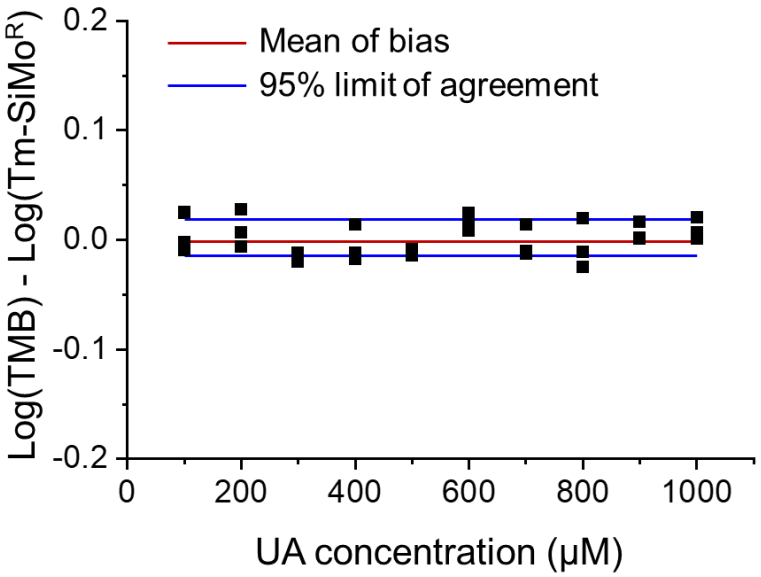

Figure 14. Bland-Altmann analysis for 30 UA buffer samples measured by Tm-SiMo^{R}-BTUO and reference TMB colorimetric assay.

The standard solutions of UA, NADPH, and PEA are prepared by dissolving analytes in phosphate buffered saline (pH = 7.4). All standard solutions are used immediately after formulation. To set up the calibration curve for UA determination, 1 mL Tm-SiMo^{R}-BTUO dispersion (1 mg mL^{-1}) is added into 1 mL UA standard solution with concentrations ranging from 100 μM to 1 mM, respectively. After incubated for 60 min, the fluorescence spectra of all samples are determined, respectively. The calibration curves for NADPH and PEA determination are obtained by a similar procedure using Tm-SiMo^{R}-YcnD and Tm-SiMo^{R}-MAO-D5, respectively. The standard colorimetric method that uses 3,3′,5,5′-tetramethylbenzidine (TMB) is used for comparison.[36]

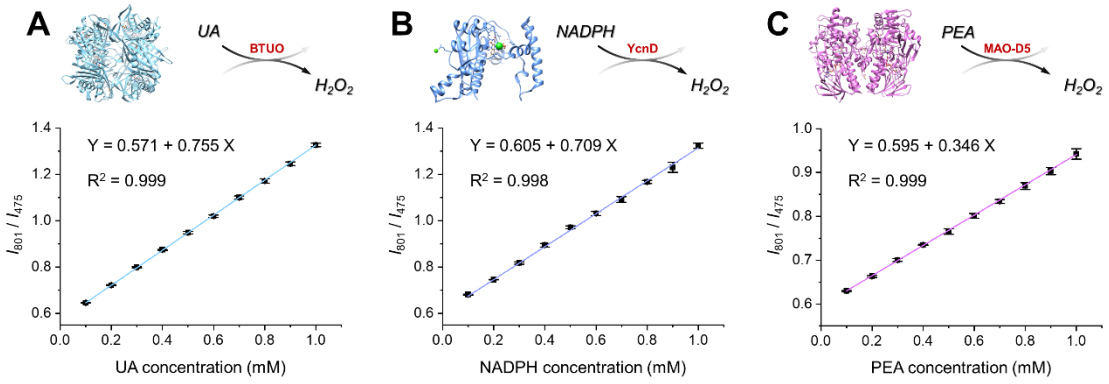

Figure 15. Calibration curves of UA by engineered UA oxidase-conjugated Tm-SiMo^{R}-BTUO (A), NADPH by NADPH oxidase-conjugated Tm-SiMo^{R}-YcnD (B), and PEA by engineered monoamine oxidase-conjugated Tm-SiMo^{R}-MAO-D5 (C). Data are presented as mean ± SD (n = 3).

3.5.12. Stability of Tm-SiMo^R-BTUO

To study the stability of Tm-SiMo^R-BTUO in a warm environment, the Tm-SiMo^R-BTUO is stored at 37 °C in solid state for 20 days. The commercial wild-type enzyme-modified probe, Tm-SiMo^R-wtUO, is tested under the same conditions for comparison. Every 2 days, 1 mL of freshly prepared UA standard solution (1 mM) is added to both Tm-SiMo^R-BTUO and Tm-SiMo^R-wtUO dispersions (1 mg mL^{-1}), respectively. To demonstrate the reliability of Tm-SiMo^R-BTUO after storage, 1 mL of freshly prepared UA standard solution (100 μM to 1 mM) is added to both freshly-prepared and stored Tm-SiMo^R-BTUO dispersions (1 mg mL^{-1}), respectively. After incubated for 60 min, the fluorescence spectra of all samples are determined.

3.5.13. Recyclability of Tm-SiMo^R-BTUO

To study the recyclability of Tm-SiMo^R-BTUO, 1 mL of freshly prepared UA standard solution (1 mM) is added to 1 mL Tm-SiMo^R-BTUO dispersion (1 mg mL^{-1}). After incubation for 60 min, the probe is separated via centrifugation (10000 rpm) and redispersed in DI water for fluorescence determination. Then, the above probe is mixed with 1 mL freshly prepared acidic ascorbate solution (pH = 6.0, 10 mM) and freshly prepared UA standard solution (1 mM) in turn, followed by incubation, separation, and fluorescence determination after each addition. This process is repeated 10 times. The absorbance at 801 nm and the ratio of fluorescence intensities at 801 nm and 475 nm (I_{801}/I_{475}) are recorded to evaluate the recycling capacity.

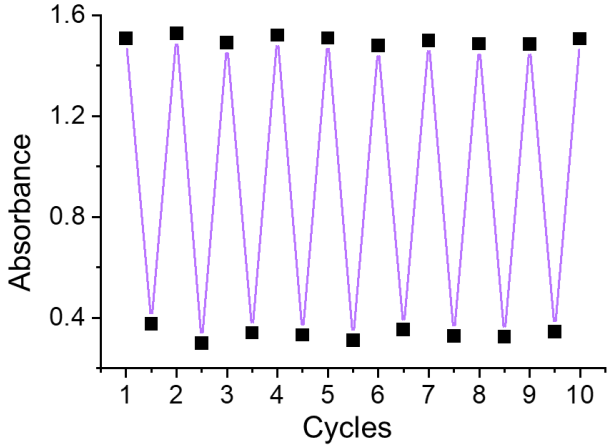

Figure 16. Absorbance of Tm-SiMoR-BTUO at 801 nm for 10 recycling processes.

3.5.14. Construction and recyclability of fluorescence assay

To construct the fluorescence assay for uric acid detection and diagnosis of hyperuricemia, 200 μL Tm-SiMo^R-BTUO dispersion (1 mg mL^{-1}) is added in each well of a 96-well plate for fluorescence determination. Then, 100 μL of sample is added in each well. After incubation for 60 min, the fluorescence in each well is determined. Then, the probes in different wells are collected and mixed in a conical flask. 5 mL of freshly prepared acidic ascorbate solution (pH = 6.0, 10 mM) is added to the mixture,

and after stirring for 30 min, the recycled probes are separated via centrifugation (10000 rpm) and redispersed in DI water. 200 µL dispersion of the recycled probe is added in each well of the same 96-well plate for fluorescence determination.

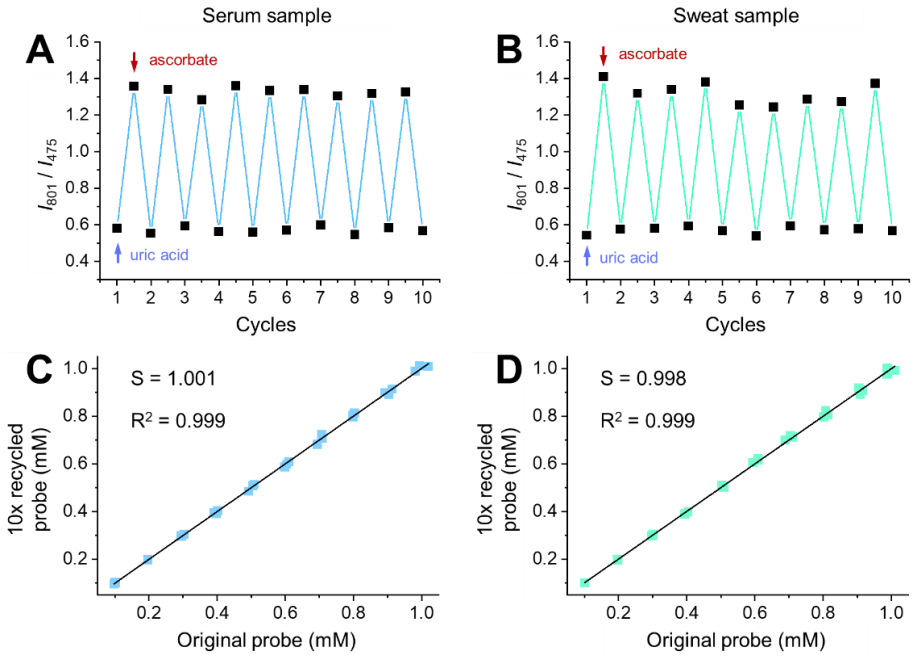

Figure 17. I_{801}/I_{475} fluorescence ratios for 10 recycling processes in simulated serum sample (A) and artificial sweat sample (B). Quantification of UA in 30 serum samples (C) and sweat samples (D). Results obtained by using 10x recycled Tm-SiMo^R-BTUO, plotted against results obtained by original Tm-SiMo^R-BTUO.

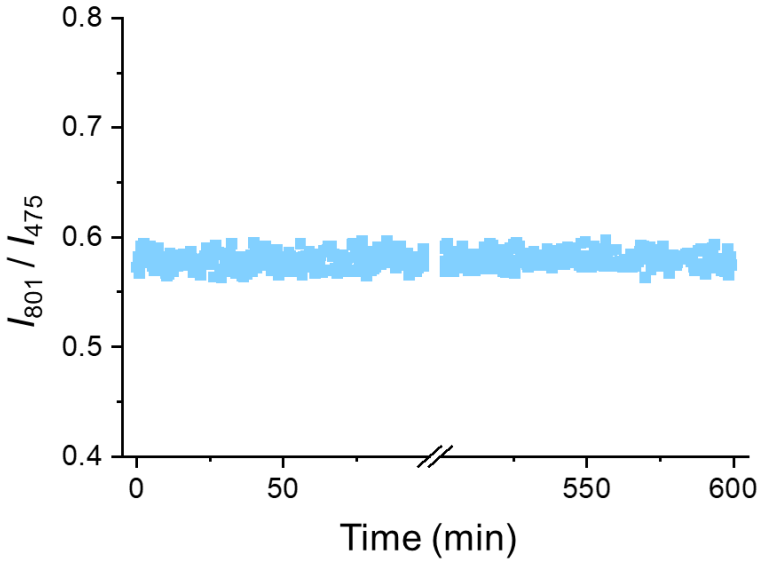

Figure 18. Photostability of I_{801}/I_{475} of Tm-SiMo^R within 600 min of laser irradiation.

3.5.15. Statistical Analysis

The fluorescence method is used to analyze 11 samples collected from normal cases and 11 samples collected from hyperuricemia cases. Receiver operating characteristic (ROC) analysis is used to determine the hyperuricemia diagnostic potential.[37] This

shows the ability to correctly differentiate normal and hyperuricemia cases by determining the UA content in artificial urine samples. The ROC analysis captures the trade-off between sensitivity and specificity while changing a discrimination threshold, but it can be summarized as a single measurement (AUC). The sensitivity (true positive rate) is plotted against the specificity (true negative rate) in the ROC curve as a function of a variety of thresholds of class prediction probabilities. The overall accuracy depends on the overlap of the output signal distributions for the two classes, in this case, UA level of normal and hyperuricemia cases. Values range between 0.5 and 1.0, where a value of 0.5 indicates that the two distributions are identical and a value of 1.0 indicates that there is no overlap in the distributions of output signals for the two classes. The AUC is used as a lone measure of evaluating the efficiency of the model ranked subjects according to the probability assigned to the positive class. The AUC of the ROC curve is calculated by the trapezoidal method of integration with the corresponding 95% confidence intervals (CI).

Table 6. I_{801}/I_{475} fluorescence ratios of original Tm-SiMo^{R}-BTUO probes in a 96-well plate, corresponding to the Figure 10B (top).

0.592	0.593	0.559	0.588	0.602	0.574	0.591	0.611	0.594	0.572	0.579	0.560
0.594	0.604	0.615	0.571	0.584	0.570	0.605	0.553	0.585	0.568	0.580	0.595
0.583	0.565	0.561	0.578	0.600	0.570	0.583	0.594	0.606	0.589	0.603	0.565
0.582	0.592	0.593	0.593	0.596	0.591	0.579	0.558	0.562	0.572	0.583	0.577
0.598	0.560	0.577	0.580	0.569	0.571	0.609	0.567	0.585	0.605	0.609	0.611
0.561	0.588	0.601	0.576	0.583	0.553	0.605	0.583	0.568	0.589	0.583	0.601
0.560	0.585	0.595	0.603	0.602	0.613	0.575	0.585	0.616	0.561	0.590	0.590
0.592	0.609	0.613	0.588	0.567	0.595	0.557	0.608	0.589	0.586	0.607	0.567

Table 7. I_{801}/I_{475} fluorescence ratios of probes after incubation with samples in a 96-well plate, corresponding to the Figure 10B (center).

0.996	1.001	0.947	0.850	0.988	0.962	0.788	1.029	0.904	0.783	0.918	0.936
1.129	0.847	0.804	0.877	0.850	0.840	0.860	0.730	0.955	0.581	0.992	0.769
0.813	0.978	0.944	0.682	0.936	0.944	0.924	0.574	0.937	0.665	0.775	1.021
1.102	0.875	0.666	0.878	0.587	0.563	0.662	0.671	0.766	0.906	0.596	1.105
0.790	0.618	0.839	0.797	0.597	0.751	0.773	0.601	0.882	0.687	0.642	0.873
1.028	0.626	0.857	0.698	0.870	0.825	0.574	0.896	0.660	0.598	0.865	0.946
0.829	0.776	0.676	0.906	0.583	0.905	0.832	0.822	0.914	0.672	0.990	0.858
1.025	0.669	0.674	0.761	0.737	0.941	0.812	0.602	0.953	0.828	0.808	0.812

Table 8. I_{801}/I_{475} fluorescence ratios of recycled probes in a 96-well plate, corresponding to the Figure 10B (bottom).

0.562	0.562	0.574	0.556	0.582	0.616	0.586	0.558	0.588	0.553	0.550	0.580
0.562	0.557	0.577	0.580	0.594	0.592	0.554	0.578	0.604	0.601	0.581	0.568
0.582	0.604	0.592	0.560	0.585	0.578	0.568	0.578	0.554	0.556	0.576	0.564
0.574	0.557	0.566	0.579	0.554	0.580	0.600	0.577	0.590	0.585	0.549	0.578
0.578	0.576	0.583	0.575	0.571	0.584	0.572	0.560	0.566	0.583	0.574	0.581
0.576	0.584	0.572	0.594	0.597	0.595	0.585	0.567	0.576	0.559	0.594	0.601
0.580	0.586	0.567	0.585	0.587	0.596	0.571	0.583	0.595	0.585	0.594	0.564
0.584	0.589	0.578	0.589	0.596	0.584	0.587	0.584	0.562	0.588	0.577	0.586

3.6. References

[1] Hannay, E., Fernandez-Suarez, M. & Duneton, P. COVID-19 diagnostics: preserving manufacturing capacity for future pandemics. *BMJ Glob. Health* **7**, e007494, https://doi.org/10.1136/bmjgh-2021-007494 (2022).

[2] Luo, R., Fong, Y., Boeras, D., Jani, I. & Vojnov, L. The clinical effect of point-of-care HIV diagnosis in infants: a systematic review and meta-analysis. *Lancet* **400**, 887-895, https://doi.org/10.1016/S0140-6736(22)01492-1 (2022).

[3] Liu, W. & Lee, L. P. Toward rapid and accurate molecular diagnostics at home. *Adv. Mater.* **35**, e2206525, https://doi.org/10.1002/adma.202206525 (2023).

[4] Ito, E., Iha, K., Yoshimura, T., Nakaishi, K. & Watabe, S. Early diagnosis with ultrasensitive ELISA. *Advan. Clin. Chem.* **101**, 121-133, https://doi.org/10.1016/bs.acc.2020.06.002 (2021).

[5] Straightforward, inexpensive and sensitive. *Nat. Biomed. Eng.* **6**, 923-924, https://doi.org/10.1038/s41551-022-00935-w (2022).

[6] Mabey, D., Peeling, R. W., Ustianowski, A. & Perkins, M. D. Diagnostics for the developing world. *Nat. Rev. Microbiol.* **2**, 231-240, https://doi.org/10.1038/nrmicro841 (2004).

[7] Auzel, F. Upconversion and anti-Stokes processes with f and d ions in solids. *Chem. Rev.* **104**, 139-173, https://doi.org/10.1021/cr020357g (2004).

[8] Zheng, W. *et al.* Lanthanide-doped upconversion nano-bioprobes: electronic structures, optical properties, and biodetection. *Chem. Soc. Rev.* **44**, 1379-1415, https://doi.org/10.1039/c4cs00178h (2015).

[9] Lv, R., Raab, M., Wang, Y., Tian, J., Lin, J. & Prasad, P. N. Nanochemistry advancing photon conversion in rare-earth nanostructures for theranostics. *Coord. Chem. Rev.* **460**, 214486, https://doi.org/ARTN 214486
10.1016/j.ccr.2022.214486 (2022).

[10] Xu, J., Gulzar, A., Yang, P., Bi, H., Yang, D., Gai, S., He, F., Lin, J., Xing, B. & Jin, D. Recent advances in near-infrared emitting lanthanide-doped nanoconstructs: Mechanism, design and application for bioimaging. *Coord. Chem. Rev.* **381**, 104-134, https://doi.org/10.1016/j.ccr.2018.11.014 (2019).

[11] All, A. H., Zeng, X., Teh, D. B. L., Yi, Z., Prasad, A., Ishizuka, T., Thakor, N., Hiromu, Y. & Liu, X. Expanding the toolbox of upconversion nanoparticles for *in vivo* optogenetics and neuromodulation. *Adv. Mater.* **31**, e1803474, https://doi.org/10.1002/adma.201803474 (2019).

[12] Gnach, A., Lipinski, T., Bednarkiewicz, A., Rybka, J. & Capobianco, J. A. Upconverting nanoparticles: assessing the toxicity. *Chem. Soc. Rev.* **44**, 1561-1584, https://doi.org/10.1039/c4cs00177j (2015).

[13] Zhou, J., Liu, Q., Feng, W., Sun, Y. & Li, F. Upconversion luminescent materials: advances and applications. *Chem. Rev.* **115**, 395-465, https://doi.org/10.1021/cr400478f (2015).

[14] Yang, Y., Chen, Y., Pei, P., Fan, Y., Wang, S., Zhang, H., Zhao, D., Qian, B. Z. & Zhang, F. Fluorescence-amplified nanocrystals in the second near-infrared window for in vivo real-time dynamic multiplexed imaging. *Nat. Nanotechnol.* **18**, 1195-1204, https://doi.org/10.1038/s41565-023-01422-2 (2023).

[15] Kamarudin, J. B. M., Sun, B., Foo, A. S. C., Lim, X. Y., Judd, H., Tan, X., Tan, X. H., Razar, R., Liu, M., Zhong, J., Chua, J. J. E., Ng, C. W. Q., Goh, J. C. H., Tan, T. Z., Parikh, B. H., Su, X., Kumar, A. P., Ong, W. Y., Yamaguchi, N., Set, S. Y., Yip, G. W., Zhang, Y. & Teh, D. B. L. SIRIUS, ultra-scintillating upconversion breast implant for remote orthotopic photodynamic therapy. *ACS Nano* **17**, 11593-11606, https://doi.org/10.1021/acsnano.3c01916 (2023).

[16] Chen, S., Weitemier, A. Z., Zeng, X., He, L., Wang, X., Tao, Y., Huang, A. J. Y., Hashimotodani, Y., Kano, M., Iwasaki, H., Parajuli, L. K., Okabe, S., Teh, D. B. L., All, A. H., Tsutsui-Kimura, I., Tanaka, K. F., Liu, X. & McHugh, T. J. Near-infrared deep brain stimulation via upconversion nanoparticle-mediated optogenetics. *Science* **359**, 679-684, https://doi.org/10.1126/science.aaq1144 (2018).

[17] Zhao, X., Yang, C. X., Chen, L. G. & Yan, X. P. Dual-stimuli responsive and reversibly activatable theranostic nanoprobe for precision tumor-targeting and fluorescence-guided photothermal therapy. *Nat. Commun.* **8**, 14998, https://doi.org/10.1038/ncomms14998 (2017).

[18] Duan, Q., He, Y., Bi, W., Liang, T., Liu, Z. & Li, Z. In vivo monitoring of hydrogen polysulfide via a NIR-excitable reversible fluorescent probe based on upconversion luminescence resonance energy transfer. *Anal. Chem.* **94**, 8792-8801, https://doi.org/10.1021/acs.analchem.2c01650 (2022).

[19] Liu, X., He, L., Gong, X., Yang, Y., Cheng, D., Peng, J., Wang, L., Zhang, X.-B. & Yuan, L. Engineering of reversible luminescent probes for real-time intravital imaging of liver injury and repair. *CCS Chem.* **4**, 356-368, https://doi.org/10.31635/ccschem.021.202000679 (2022).

[20] Liu, Y., Jia, Q., Guo, Q., Jiang, A. & Zhou, J. In vivo oxidative stress monitoring through intracellular hydroxyl radicals detection by recyclable upconversion nanoprobes. *Anal. Chem.* **89**, 12299-12305, https://doi.org/10.1021/acs.analchem.7b03270 (2017).

[21] Xiao, Q., Zheng, X., Bu, W., Ge, W., Zhang, S., Chen, F., Xing, H., Ren, Q., Fan, W., Zhao, K., Hua, Y. & Shi, J. A core/satellite multifunctional nanotheranostic for in vivo imaging and tumor eradication by radiation/photothermal synergistic therapy. *J. Am. Chem. Soc.* **135**, 13041-13048, https://doi.org/10.1021/ja404985w (2013).

[22] Liu, B., Li, C., Ma, P., Chen, Y., Zhang, Y., Hou, Z., Huang, S. & Lin, J. Multifunctional NaYF4:Yb, Er@mSiO_2@Fe_3O_4-PEG nanoparticles for UCL/MR bioimaging and magnetically targeted drug delivery. *Nanoscale* **7**, 1839-1848, https://doi.org/10.1039/c4nr05342g (2015).

[23] Yuan, P., Lee, Y. H., Gnanasammandhan, M. K., Guan, Z., Zhang, Y. & Xu, Q. H. Plasmon enhanced upconversion luminescence of $NaYF_4$:Yb,Er@SiO_2@Ag core-shell nanocomposites for cell imaging. *Nanoscale* **4**, 5132-5137, https://doi.org/10.1039/c2nr31241g (2012).

[24] Li, J., Yao, S., Song, S., Wang, X., Wang, Y., Ding, X., Wang, F. & Zhang, H. Designed synthesis of multi-functional PEGylated Yb_2O_3:Gd@SiO_2@CeO_2 islands core@shell nanostructure. *Dalton Trans.* **45**, 11522-11527, https://doi.org/10.1039/c6dt02044e (2016).

[25] Liu, Y., Zhu, X., Wei, Z., Feng, W., Li, L., Ma, L., Li, F. & Zhou, J. Customized photothermal therapy of subcutaneous orthotopic cancer by multichannel luminescent nanocomposites. *Adv. Mater.* **33**, e2008615, https://doi.org/10.1002/adma.202008615 (2021).

[26] Liu, Y., Zhu, X., Wei, Z., Wu, K., Zhang, J., Mutti, F. G., Zhang, H., Loeffler, F. F. & Zhou, J. Multi-channel lanthanide nanocomposites for customized synergistic treatment of

orthotopic multi-tumor cases. *Angew. Chem. Int. Ed.* **62**, e202303570, https://doi.org/10.1002/anie.202303570 (2023).

[27] Hibi, T., Kume, A., Kawamura, A., Itoh, T., Fukada, H. & Nishiya, Y. Hyperstabilization of tetrameric *Bacillus sp.* TB-90 urate oxidase by introducing disulfide bonds through structural plasticity. *Biochemistry* **55**, 724-732, https://doi.org/10.1021/acs.biochem.5b01119 (2016).

[28] Morokutti, A., Lyskowski, A., Sollner, S., Pointner, E., Fitzpatrick, T. B., Kratky, C., Gruber, K. & Macheroux, P. Structure and function of YcnD from *Bacillus subtilis*, a flavin-containing oxidoreductase. *Biochemistry* **44**, 13724-13733, https://doi.org/10.1021/bi0510835 (2005).

[29] Knaus, T., Cariati, L., Masman, M. F. & Mutti, F. G. In vitro biocatalytic pathway design: orthogonal network for the quantitative and stereospecific amination of alcohols. *Org. Biomol. Chem.* **15**, 8313-8325, https://doi.org/10.1039/c7ob01927k (2017).

[30] Dunsmore, C. J., Carr, R., Fleming, T. & Turner, N. J. A chemo-enzymatic route to enantiomerically pure cyclic tertiary amines. *J. Am. Chem. Soc.* **128**, 2224-2225, https://doi.org/10.1021/ja058536d (2006).

[31] Batista, V. F., Galman, J. L., Pinto, D. C. G. A., Silva, A. M. S. & Turner, N. J. Monoamine Oxidase: Tunable Activity for Amine Resolution and Functionalization. *ACS Catal.* **8**, 11889-11907, https://doi.org/10.1021/acscatal.8b03525 (2018).

[32] Sarigul, N., Korkmaz, F. & Kurultak, I. A new artificial urine protocol to better imitate human urine. *Sci. Rep.* **9**, 20159, https://doi.org/10.1038/s41598-019-56693-4 (2019).

[33] Possanzini, L., Decataldo, F., Mariani, F., Gualandi, I., Tessarolo, M., Scavetta, E. & Fraboni, B. Textile sensors platform for the selective and simultaneous detection of chloride ion and pH in sweat. *Sci. Rep.* **10**, 17180, https://doi.org/10.1038/s41598-020-74337-w (2020).

[34] Liu, Y., Guo, Q., Zhu, X., Feng, W., Wang, L., Ma, L., Zhang, G., Zhou, J. & Li, F. Optimization of prussian blue coated $NaDyF_4$:x%Lu nanocomposites for multifunctional imaging‐guided photothermal therapy. *Adv. Funct. Mater.* **26**, 5120-5130, https://doi.org/10.1002/adfm.201601478 (2016).

[35] Liu, Y., Zhu, X., Wei, Z., Wu, K., Zhang, J., Mutti, F. G., Zhang, H., Loeffler, F. F. & Zhou, J. Multi-channel lanthanide nanocomposites for customized synergistic treatment of orthotopic multi-tumor cases. *Angew. Chem. Int. Ed.*, e202303570, https://doi.org/https://doi.org/10.1002/anie.202303570 (2023).

[36] Vashist, S. K. & Luong, J. H. T. in *Handbook of Immunoassay Technologies* (eds Sandeep K. Vashist & John H. T. Luong) 97-127 (Academic Press, 2018).

[37] Liu, Y., Wei, Z., Zhou, J. & Ma, Z. Simultaneous multi-signal quantification for highly precise serodiagnosis utilizing a rationally constructed platform. *Nat. Commun.* **10**, 5361, https://doi.org/10.1038/s41467-019-13358-0 (2019).